Advances in Met S&T 气象科技进展

Applications of Special Sensor Microwave Imager and Sounder (SSMIS) Measurements in Weather and Climate Studies

Weng F[1,2], Zou X*[3,4], Yan B[2], Han Y[1,2], Liu Q[2,5]

(1 NOAA/NESDIS/Center for Satellite Applications and Research, USA 2 Joint Center for Satellite Data Assimilation, USA 3 NUIST Center of Data Assimilation for Research and Application, China 4 Department of Earth, Ocean and Atmospheric Sciences, Florida State University, USA 5 IMSG, Inc, USA)

Abstract: On October 18, 2003, the Defense Meteorological Satellite Program (DMSP) successfully launched the F–16 satellite with the Special Sensor Microwave Imager/Sounder (SSMIS) on board. However, this first SSMIS instrument exhibited several major measurement anomalies due to instabilities in its antenna emission and calibration target. Two algorithms have been developed at Naval Research Laboratory (NRL) and the National Oceanic and Atmospheric Administration (NOAA), respectively, for correcting for these anomalies. After removal of the calibration anomalies, SSMIS data are now much more useful for sounding product retrievals and data assimilation. NOAA generates SSMIS imager products from its legacy SSM/I algorithms. Several new algorithms have been developed to extract from SSMIS the information on clouds and precipitation. In the cloud ice water retrieval algorithm, a parametric relationship relates brightness temperatures to cloud ice water path and particle mean diameter. Atmospheric temperature and water vapor profiles are simultaneously retrieved along with cloud hydrometeor profiles through a one–dimensional variational (1D–Var) retrieval system, which works well under most atmospheric and surface conditions. Root–mean–square (RMS) errors of temperature and water vapor profiles from SSMIS are typically 2K and 15%, respectively, under all weather conditions. A new quality control algorithm and a bias correction algorithm have also been developed for SSMIS data assimilation. Assimilation of SSMIS data in the NOAA Global Forecast System (GFS) results in neutral and small positive impacts on global medium range forecast scores.

1 Introduction

In the past two decades, space-borne microwave radiometers have progressed from early demonstrations of both engineering feasibility and geophysical-retrieval performance to direct operational applications in weather and climate studies. Many successful applications can be attributed to the Special Sensor Microwave Imagers (SSM/I), initially launched in 1987 onboard the first of a series of Defense Meteorological Satellite Program (DMSP) satellites, and the Advanced Microwave Sounding Units (AMSU), first launched onboard NOAA-15 in July, 1998. The SSM/I contains six channels in window regions (19.35, 37.0, 85 GHz) between atmospheric absorption bands with dual polarizations, and a channel centered on 22.235 GHz with only vertical polarization. From SSM/I observations, a number of products including rainfall, snow-cover, cloud liquid water, water vapor, sea surface wind, sea ice concentration, and snow and sea ice emissivity have been developed and made operational to weather and climate communities[1]. The AMSU measures brightness temperatures at 20 channels ranging from 22.235 to 183 GHz. From the AMSU measurements, atmospheric temperature and water vapor profiles are also derived in addition to SSM/I-like products. Thus, a combination of AMSU and SSM/I measurements offer global observations with much improved temporal and spatial information.

On October 18, 2003, DMSP successfully launched the F-16 satellite with SSMIS on board. The SSMIS replaces the legacy sensors on the previous DMSP spacecraft: the SSM/I, the Special Sensor Microwave/Temperature (SSM/T) and the Special Sensor Microwave/Water Vapor (SSM/T2). This instrument provides temperature soundings up to 100 km in altitude in addition to water vapor soundings and SSM/I type data. The SSMIS, which will fly on the DMSP F-16 through F-20 satellites, is becoming a vital component of the polar-orbiting satellite constellation of the next decade along with the NOAA-EUMETSAT Joint Polar Satellite System (IPSS) (formerly National Polar-orbiting Environmental Satellite System, NPOESS). F-17 and F-19, especially, will provide unique atmospheric sounding from their early morning orbits at 5:30am while NOAA and METOP satellites will cover the afternoon and mid-morning orbits, respectively.

In the past 20 years, NOAA has accumulated extensive experience in the operational applications of satellite microwave measurements. Since the 1990s, NOAA has maintained a continual involvement in the DMSP program, participating on the SSM/I calibration and validation (Cal/Val) team and delivering several versions of SSM/I algorithms to the Fleet Numerical Meteorology and Oceanography Center (FNMOC) for operational implementation[2,3]. NOAA's National Environmental Satellite, Data, and Information Service (NESDIS) has routinely produced monthly SSM/I products from 1987, which are archived at National Climate Data Center (NCDC) [1]. These activities will be continued and expanded to generate not only the retrieval products from SSMIS, but also

收稿日期：2011年5月18日；修回日期：2011年5月29日
通讯作者：Zou X , Email:xzou@fsu.edu

the end-to-end responsibility for radiance calibration, product developments, and data assimilation into weather and climate models. NESDIS is responsible for developing enhanced products from operational satellites to meet user requirements from NOAA and international communities. This overview summarizes the recent SSMIS research and development activities at NOAA/NESDIS.

2 Special Sensor Microwave Imager and Sounder (SSMIS)

2.1 Instrumentation

The US Defense Meteorology Satellite Program (DMSP) F-16 satellite was launched successfully on October 18, 2003. On board F-16, the SSMIS measures the Earth's radiation at 24 channels (see Table 1) from 19.35 to 183 GHz and scans conically at a 53-degree earth incident angle (see Figure 1).

The objective of the SSMIS was to provide improved atmospheric temperature and water vapor sounding under all-weather conditions by configuring imaging and sounding channels with the same viewing geometry and allow for a simultaneous retrieval of surface parameters with a uniform spatial resolution across the scan swath. As shown in Fig. 1a, the upper atmospheric sounding is extended to 100 km altitude. Compared with the previous SSM/I instrument on board F-8 to F-15 satellites, SSMIS scan swath increases from approximately 1400 km to 1700 km, thus offering much fewer orbit gaps from the 833 km spacecraft altitude.

SSMIS brightness temperatures from the Earth scene are derived from a satellite microwave radiometer through a series of instrument calibration steps. First, a raw receiver voltage count is converted to an antenna-beam-averaged temperature using a calibration equation that requires measurements from warm and cold calibration targets[5].

This antenna temperature is then converted to the main-beam-referenced brightness temperature where the side-lobe contribution is removed. For SSMIS polarization channels, an additional correction is made for a spill-over effect from the cross-polarization leakage. Thus, any remaining errors in antenna brightness temperature (temperature data record or TDR) will be translated into sensor brightness temperature (sensor data record or SDR) during the calibration process.

Table1. Characteristics of SSMIS channels

Channel	Center Freq. (GHz)	3-db Width (MHz)	Freq. Stab. (MHz)	Pol.	NEΔT (K)	Sampling Interval(km)
1	50.3	380	10	H	0.34	37.5
2	52.8	389	10	H	0.32	37.5
3	53.596	380	10	H	0.33	37.5
4	54.4	383	10	H	0.33	37.5
5	55.5	391	10	H	0.34	37.5
6	57.29	330	10	RCP	0.41	37.5
7	59.4	239	10	RCP	0.40	37.5
8	150	1642(2)	200	H	0.89	12.5
9	183.31+/-6.6	1526(2)	200	H	0.97	12.5
10	183.31+/-3	1019(2)	200	H	0.67	12.5
11	183.31+/-1	513(2)	200	H	0.81	12.5
12	19.35	355	75	H	0.33	25
13	19.35	357	75	V	0.31	25
14	22.235	401	75	V	0.43	25
15	37	1616	75	H	0.25	25
16	37	1545	75	V	0.20	25
17	91.655	1418(2)	100	V	0.33	12.5
18	91.655	1411(2)	100	H	0.32	12.5
19	63.283248+/-0.285271	1.35(2)	0.08	RCP	2.7	75
20	60.792668+/-0.357892	1.35(2)	0.08	RCP	2.7	75
21	60.792668+/-0.357892+/-0.002	1.3(4)	0.08	RCP	1.9	75
22	60.792668+/-0.357892+/-0.0055	2.6(4)	0.12	RCP	1.3	75
23	60.792668+/-0.357892+/-0.016	7.35(4)	0.34	RCP	0.8	75
24	60.792668+/-0.357892+/-0.050	26.5(4)	0.84	RCP	0.9	37.5
Notes	(1) Sampling refers to along-scan direction based on 833km spacecraft altitude. (2) NEΔT for instrument temperature 0C and calibration target 260K with integration times of 8.4 msec for Channels 12-16; 12.6 msec for Channels 1-7, 24; and 25.2 msec for Channels 19-23 and 4.2 msec for Channels 8-11, 17-18. (3) Number of sub-bands is indicated by (n) next to individual 3-db width. (4) RCP denotes right-hand circular polarization. (5) Channel 1-5 (LAS) were incorrectly designed as V-POL on F-16. All other SSMIS Flight units will be configured as H-POL.					

2.2 Radiance Anomalies

Several anomalies showed up in the F-16 SSMIS TDR data for all channels, which resulted primarily from thermal emission of the main reflector as well as a perturbation in calibration target count[6]. Similar anomalies are also observed in SSMIS SDR data. These anomalies can severely downgrade the

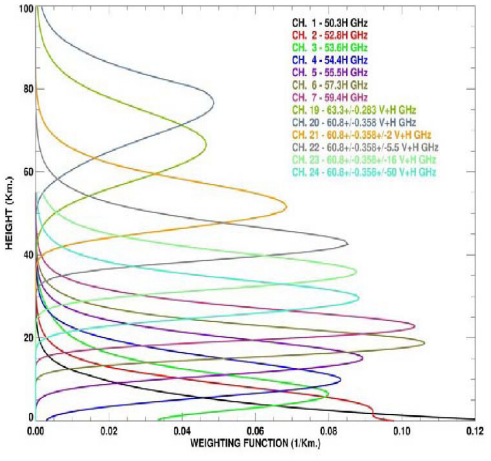

Figure 1a: SSMIS weighting functions for a standard atmosphere (from [4]).

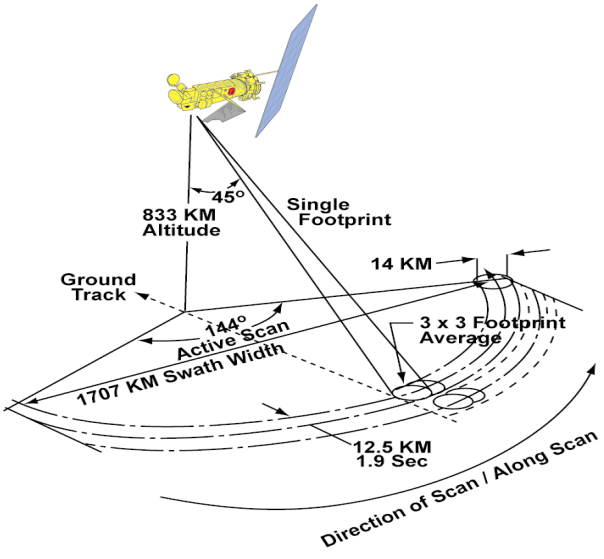

Figure 1b: SSMIS scan geometry (from [4]).

usefulness of SSMIS measurements in various environmental applications. Figure 2 displays the biases of SSMIS observations to simulations at 54.4 GHz, where the simulations are calculated using the temperature and water vapor profiles from the National Center for Environmental Prediction (NCEP) GFS Data Assimilation System (GDAS). Normally, the biases should be fairly uniform when the simulated brightness temperatures at microwave sounding channel are compared to the observations from NOAA and METOP satellites. Here, the bias varies with latitude on the order of several degrees in Kelvin.

The causes for these anomalies to occur have been investigated by the SSMIS instrument calibration team since the instrument was launched. It is found to be mainly due to the emission of the main reflector, as well as the direct solar and stray light contamination on two calibration targets[6]. It has also been shown that the SSMIS on the F-17 satellite, which was launched in November 2006, has even larger reflector emission, on the order of 1.5-2 K at 50-60 GHz and 5-8 K at 183 GHz[7]. According to Swadley et al.[7], the newest SSMIS instrument on board F18, which was launched in October 2009, performs much better since its main reflector has minimal emission, on the order of 0.5K for most of the sounding channels. The global bias distribution is also fairly stable and uniform.

The SSMIS antenna and calibration subsystem consists of a main reflector, six corrugated feedhorns, a warm calibration load and a sub-reflector for viewing cold space. In each scan, the radiation from the Earth's atmosphere is focused via the main reflector to the feedhorns and then to the receiver subsystem. At the end of the scan, the feedhorns also pass beneath a stationary warm load and cold space reflector, providing periodic calibration of the measured earth-viewing radiances as the input to the feedhorns. The receiver subsystem accepts the energies from the six feedhorns and provides amplification, filtering, and additional frequency multiplexing to output 24 discrete frequency bands to the signal processing subsystem. Then, the received scene count of the earth-viewing radiance is converted to antenna temperature (scene temperature) by a calibration

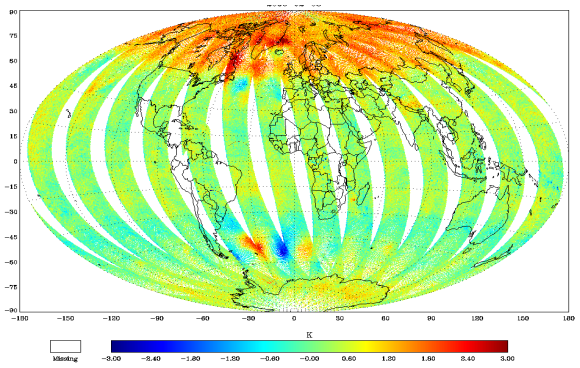

Figure 2: Bias of F-16 SSMIS brightness temperatures with respect to model simulations at 54.4 GHz. The inputs for simulations are based on GFS analysis fields.

equation, which makes use of the temperatures and counts of two calibration targets. Thus, the emission from the main reflector and the solar heating on the calibration targets can both result in the anomalies in the SSMIS antenna temperatures.

2.3 Anomaly Correction Algorithm

NESDIS developed an algorithm to correct SSMIS anomalies at the TDR level, including predicting the reflector face temperature, and detecting and removing the warm target calibration count anomalies[8]. Essentially, the total energy in terms of antenna brightness temperature received at the feedhorns is

$$T_A^{'} = T_A + \varepsilon_R (T_R - T_A), \quad (1)$$

where T_A is the antenna brightness temperature corresponding to the Earth scene temperature, and T_R the reflector face temperature. If the reflector emissivity, ε_R, and face temperature are known, T'_A can be calculated. From the NRL antenna model, the emissivity of the main reflector is given as 0.012, 0.016, 0.020, 0.025, and 0.035 at 19.35, 37, 60, 91.65 and 183 GHz, respectively, for vertically polarized channel at an incidence angle of 20 degrees[6]. The reflector face temperature is estimated from the antenna arm temperatures[8,9].

The locations of SSMIS warm target anomalies are detected through the Fast Fourier Transform (FFT) analysis on one orbit of calibration target information (warm count and platinum resistance thermometer (PRT) temperature[10]). From a linear algorithm, the anomaly in antenna brightness temperature can be expressed as

$$\Delta T_A = -\frac{T_A - T_C}{C_W - C_C}\Delta C_W - \frac{T_W - T_A}{C_W - C_C}\Delta C_C + \frac{C_S - C_C}{C_W - C_C}\Delta T_W. \quad (2)$$

where ΔC_W, ΔC_C, ΔT_W are jumps in warm and cold counts, PRT temperature. T_A, T_C and T_W are temperatures of scene target, cold space target, and warm load target. Thus, for solar heating, the warm target count anomaly is positive and depresses the antenna temperature whereas the PRT temperature anomaly is also positive and increases the antenna temperature. Temperature anomalies from warm counts (ΔC_W) could contribute to antenna brightness temperature anomaly (ΔT_A) from -0.5 to -1.5 K at most for all channels. Among the three anomalous increments (ΔC_W, ΔC_C, ΔT_W), ΔC_W dominates and depresses the SSMIS antenna temperatures for most channels.

The antenna emission and the calibration target anomaly are important error sources that produce the anomalous SSMIS radiances over most of the globe. The antenna emission occurs at all channels all over the global, but it becomes significant(1 ~ 3 K) at high latitudes in the Northern Hemisphere where the solar heating on the main reflector is the highest. Among the calibration target anomalies, the warm load count anomaly is most noticeable and it alone can depress the SSMIS temperature by about 1 K. The warm load count anomaly occurs only over several latitudinal bands, but it affects almost all channels. More importantly, the location and magnitude of the emission and calibration target anomalies vary with season.

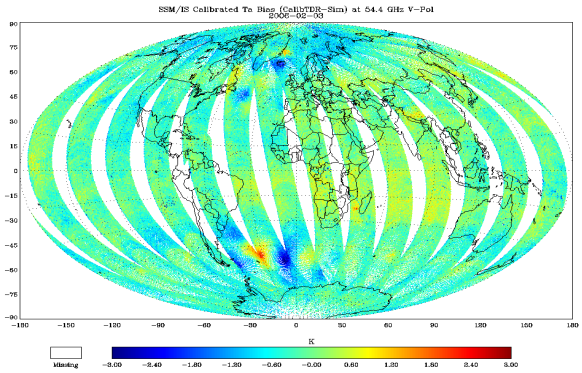

Figure 3: Same as Fig. 2 except with the anomaly correction.

The antenna temperatures after applying the SSMIS anomaly correction are evaluated at 54.4, 55.5, 57.3, and 59.4 GHz. Figure 3 displays an example of the bias of the SSMIS antenna brightness temperature at 54.4 GHz from simulations for March 20, 2005. Compared to SSMIS TDR data in Fig. 2, the antenna temperature anomalies are significantly reduced with typical biases less than 0.5 K over most of the globe. The simulations are based on the NCEP GDAS. Some of the remaining biases may be attributed to inaccurate simulations.

3 SSMIS Product Demonstration

3.1 Lower Atmospheric Sounding Products

As shown in Fig. 1, SSMIS has seven channels that are directly sensitive to tropospheric temperature distribution. Since the measurements are made from a constant satellite viewing angle, it is possible to directly see the horizontal temperature gradients without performing the retrievals. In the case of a hurricane event, SSMIS 54.4 GHz serves as an ideal tool for the warm core feature near 200 hPa[11,12]. The magnitude of this warm core is well correlated with hurricane intensity. Figure 4 corresponds to warm core evolution of Hurricane Katrina in 2005. Note that the warm core gradually strengthened prior to landfall and rapidly spreading and then weakened after landfall. The brightness temperature at the center of the hurricane in the upper-right panel (a) is about 2 degrees warmer than ambient observations. The brightness temperature is about 7.5 degrees warmer than its environment when the hurricane achieves categories 4 on the Saffir-Simpson scale (see b – d in Figure 4). Even after Katrina was downgraded to a tropical depression, the brightness temperature near the storm center was still about 2 degrees warmer than its environment due to the condensation of water vapor into clouds.

Tropospheric temperature and moisture profiles can be retrieved from SSMIS using its lower atmospheric sounder (LAS) channels. Liu and Weng[13] recently proposed a multi-step variational algorithm that retrieved temperature, moisture and cloud profiles in all-weather conditions. NCEP forecasts are used as background, and regression-based algorithms are used to produce the first guess temperature and humidity profiles. Surface wind and pressure are also taken from the NCEP forecast data. The integrated amount of cloud liquid water was found to be consistent with the original value but the profile showed differences due to the limited information content. To constrain the problem and make the retrieval more stable, hydrometeor profiles were modeled in an oversimplified fashion. The stability and ill-posed nature of the problem are two classical issues facing this type of retrieval. Boukabara et al.[14] have upgraded Liu and Weng's study[13] to handle issues related to stability and information content through empirically orthogonal function (EOF) decomposition, which also removes the need of a multi-step approach. A 1D-Var retrieval system is developed to perform simultaneous retrievals of atmospheric constituents and surface parameters in all-weather conditions, which are independent of NWP model outputs. Such a consistent treatment of all components that have an impact on the measurements allows for an optimal extraction of information content from measurements. The retrieval of the precipitating and non-precipitating cloud parameters is carried out in a profile form, taking advantage of the natural correlations that do exist between different parameters and across the vertical layers. The use of EOF decomposition leads to a dramatic stabilization of the problem.

The radiances, before being digested into the 1D-Var system, are bias-corrected. This correction removes potential inconsistencies between measurements and the forward model. A set of different coefficients is generated for every sensor. The coefficients are also generated for different scan positions (or angles for the case of cross-track sensors) to account for any scan asymmetry anomalies. The approach used to compute these biases relies on comparisons between simulations and measurements of brightness temperatures. The simulated radiances in this case use the Community Radiative Transfer Model (CRTM) forward model and take inputs from the ECMWF global analyses, interpolated in time and space to the specific locations of the measurements. These comparisons are done exclusively over ocean because the emissivity over non-ocean surfaces is not known, which limits the possibility to determine biases for surface-sensitive channels. Over ocean, the surface wind speed and emissivity model FASTEM-3[15] is used for calculating emissivity values, which are combined with atmospheric parameters from the analyses to generate brightness temperature simulations. In addition to biases, these comparisons are also used to generate estimates of radiative transfer model (RTM) uncertainties, via the standard deviation of the radiance comparisons, scaled down to account for uncertainties in the geophysical inputs themselves.

Validation of temperature and water vapor profiles is undertaken routinely at NOAA by comparing satellite retrievals with radiosonde data and NWP analysis outputs[14]. For SSMIS, the retrieval errors are stratified by land and oceans at various pressure levels and a statistical summary of the errors from several thousand of radiosondes are shown in Table 2. Notice

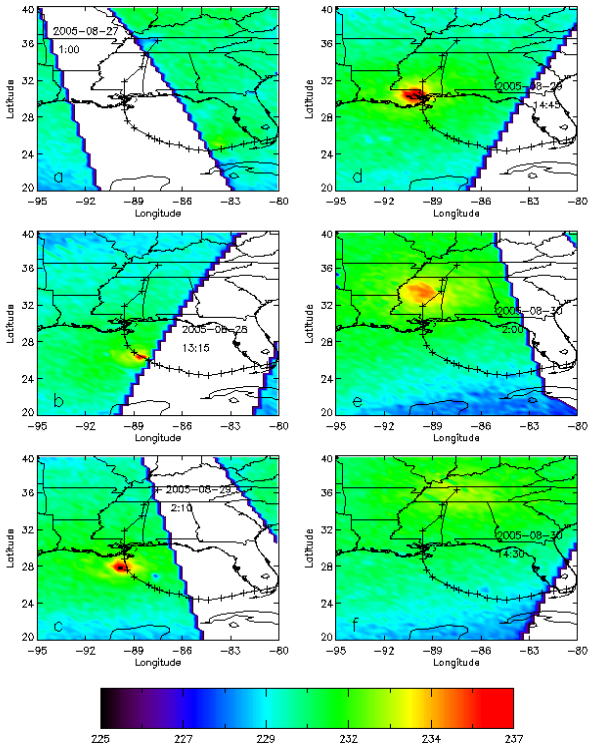

Figure 4: The observed SSMIS brightness temperatures at 54.4 GHz for hurricane Katrina in 2005 at (a) 0100 UTC August 27, (b) 1315 UTC August 28, (c) 0210 UTC August 29, (d) 1445 UTC August 29, (e) 0200 UTC August 30, (f) 1430 UTC August 30, 2005. The best track is indicated by "+" at 6-h interval.

that while the biases of SSMIS temperature retrievals are similar over land and oceans, the standard deviation is lower over oceans than that over land. For water vapor retrievals, the uncertainties are much larger. In general, microwave retrievals of water vapor profiles have errors much larger than the NPOESS Integrated Operational Requirements Document requirements. This is mainly because we have very limited channels (2-3 independent pieces of information on tropospheric water vapor), the detailed water vapor structures cannot be accurately resolved from the current microwave sounding system.

3.2 Upper Atmospheric Sounding Products

SSMIS measurements from its upper atmospheric sounding channels are used to obtain accurate stratospheric temperatures. The peaks of the weighting functions at SSMIS channels 22, 23, 24, 7, 6, and 5 approximately locate at 2, 5, 15, 30, 60, and 90 hPa, respectively. These weighting function peaks are rarely changed because the absorption of these oxygen channels for the conical scanning (constant viewing angle) sensor depends mostly on the pressure. Thus, the changes in SSMIS channel brightness temperatures approximately reflect the variations of the stratospheric temperatures. Liu and Weng[13]applied a linear regression to derive the retrieval coefficients by minimizing the difference between the predicted regression algorithm temperatures and the input temperatures. Model results show

Table 2. Statistical summary of errors (biases or accuracy, and standard deviation or precision) of SSMIS temperature and water vapor profiles at five representative pressure levels.

Pressure Level (hPa)	SSMIS temperature retrieval error components				SSMIS water vapor retrieval error components			
	Bias (Ocean)	Standard Deviation (Ocean)	Bias (Land)	Standard Deviation (Land)	Bias (Ocean)	Standard Deviation (Ocean)	Bias (Land)	Standard Deviation (Land)
100	-1.62	1.55	-1.30	1.82	5.0	58.0	-8.5	78.0
300	-0.95	2.19	0.50	1.90	48.0	79.0	16.0	77.5
500	1.20	1.61	-0.45	1.81	3.0	62.5	-2.0	57.5
800	0.25	2.20	1.10	3.05	4.0	33.5	-5.0	36.5
950	-0.25	3.12	2.25	3.70	-5.5	22.0	-15.0	34.5

that the regression algorithm can provide atmospheric temperatures at 10, 30, 50, 70, and 100 hPa with a root mean square error of less than 1 K. Figure 5 shows the time series of the temperatures at 10, 30, 50, and 70 hPa, respectively. The green, red, and black lines represent the radiosonde, retrieval using real SSMIS measurements, and NCEP analysis, respectively. As shown in Fig. 5, radiosondes, SSMIS retrievals and NCEP analyses agree in general. The stratospheric temperatures at 10, 30, 50, and 70 hPa reach a minimum in June, July, August, and September, respectively. In Fig. 5a, the retrieval and NCEP analysis agree well. The small difference in the temperature at 30 hPa in spring and summer among radiosondes, retrievals, and analyses can be observed. At 50 and 70 hPa, all three datasets, radiosonde, retrieval, and NCEP analysis, agree well (see Figs, 5c and 5d). The results show that radiosonde data are in general reliable, but strict quality control for radiosonde measurements at/above 10 hPa may be necessary. The retrieval of the stratospheric temperature can be easily carried out and the retrieval product may be used for quick monitoring of the stratospheric temperature.

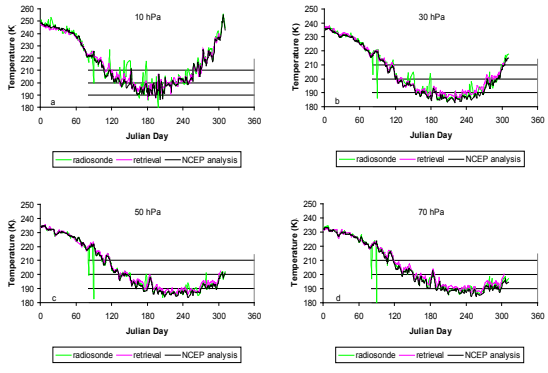

Figure 5: Temporal variations of the stratospheric temperatures in 2006 at Van Neumayer station from The Green, red, and black lines represent radiosondes (green), SSMIS retrievals (red), and NCEP operational analyses (black), respectively.

3.3 Imager and Environmental Products

As shown in Table 1, SSMIS imager measurements are those from channels 12-18 and the environmental observations are those from channels 8 to 11. Since several operational agencies such as NESDIS and FNMOC continue running SSM/I algorithms for SSMIS imaging products, we first apply linear mapping algorithm to convert SSMIS imaging channels from

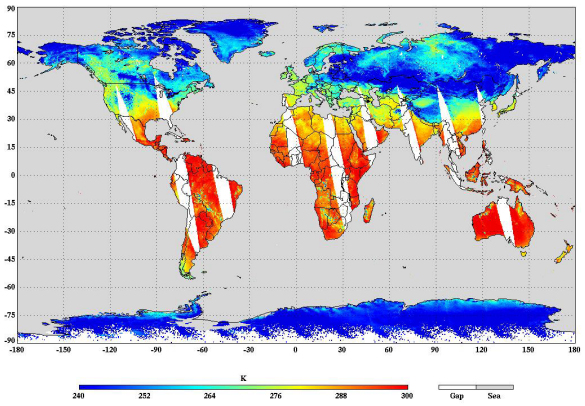

Figure 6: F-16 SSMIS derived global land surface temperature at 1908 UTC January 20, 2010.

19.35, 22.235, 37, 91.665 GHz to SSM/I-like channels. The coefficients for this linear mapping are kindly provided by Mr. Steve Swadley at NRL. The mapping will statistically make all SSMIS window channels (e.g. 19.35VH, 22.235V, 37VH, 91.665VH) the same as SSM/I channels. In addition, we also use the antenna pattern correction coefficients (APC) from NRL to correct some spill-over effects from the antenna side lobe. After these corrections, SSMIS products are produced with a quality similar to SSM/I.

Since SSM/I-like products were discussed and presented in many previous publications[2,3,16,17], here several newly developed algorithms are further presented. The land surface temperature (LST) algorithm for SSM/I was originally presented using only the two lowest SSM/I channels at 19.35 and 22.235 GHz[18]. Recently, more SSM/I channels are used to improve the performance. LST can be easily obtained over a variety of land surface conditions[19]. The SDR measurements at 22.235 GHz V, 37.0 GHz V and 85.5 GHz V are used in this algorithm as shown by the following equation:

$$\begin{aligned} LST = \; & 0.02509[1.7167 - 0.005514(TB_{22v})]TB_{22v} \\ & -[0.1083 + 0.001976(TB_{37v})]TB_{37v} \\ & +[1.1763 - 0.000636(TB_{85v})]TB_{85v} \end{aligned} \quad (3)$$

The global retrieved LST is shown in Fig. 6. Notice that most of Eurasia has a lower LST due to the snow cover. Overall, the SSM/I LST retrieval algorithm may be migrated to SSMIS for operational use but there is still a need to refine the remapping coefficients that convert SSMIS brightness temperatures at 91.655 GHz to SSM/I brightness temperature at 85.5 GHz, since Eq. (3) is used for both SSM/I and SSMIS.

The land emissivity is an important parameter that can be used to infer some other geophysical parameters, such as soil moisture, vegetation water and soil wetness. For low frequency channels at 19.35 GHz V/H and 37 GHz V/H, their emissivity is based on a linear regression relationship among all seven SSM/I-like channel SDR measurements, shown in the following equation

$$\begin{aligned} \varepsilon = \; & a_0 + a_1(TB_{19v}) + a_2(TB_{19h}) + a_3(TB_{22v}) \\ & a_4(TB_{37v}) + a_5(TB_{37h}) + a_6(TB_{85v}) + a_7(TB_{85h}) \end{aligned} \quad (4)$$

For emissivity at 85V and 85H, a nonlinear relation is built from 37.0 GHz V and 85.5 GHz V/H by

$$\begin{aligned} \varepsilon = \; & b_0 + [b_1 + b_2(TB_{37v})](TB_{37v}) \\ & [b_3 + b_4(TB_{85v})](TB_{85v}) + [b_5 + b_6(TB_{85h})](TB_{85h}) \end{aligned} \quad (5)$$

where the coefficients for the emissivity retrievals in eqs. (4) and (5) are available and shown in Table 3. Figure 7 shows an example of the land emissivity at 37 GHz for a vertical polarization. Overall, the snow surface has much lower emissivity than those of other surfaces.

From the SSMIS highest frequencies, cloud microphysical parameters can be observed at a spatial resolution of 15 km. In our previous studies[20,21], a simplified two-stream radiative transfer model is applied for microwave applications so that a three-parameter equation can be derived to link the ice cloud water path (IWP), ice particle effective diameter (De) and bulk volume density. Since SSMIS is a conically-scanning instrument, the retrieved IWP is less dependent on scan position and is an ideal product for imaging atmospheric ice-phase clouds related to precipitation. The SSMIS derived ice cloud products are compared to those by different algorithms from other instruments and agree well in the spatial distributions[19]. Figure 8 displays a retrieval of cloud ice water path for Hurricane Gustav. Gustav was one of the most destructive hurricanes of the 2008 Atlantic hurricane season. It caused serious damage and casualties in several countries in the Caribbean and triggered the largest evacuation in the United States history. Gustav formed on August 25, 2008 southeast of Haiti, and rapidly strengthened into a tropical storm that afternoon and into a hurricane early the next day. Note that the hurricane eyewall and spiral rainfall bands are associated with large IWP of more than 2. The maximum IWP bands exist at the southern section of the

Table 3. Coefficients used for emissivity retrievals

Channel	a_0	a_1	a_2	a_3	a_4	a_5	a_6	a_7
19.35 V	0.5098	4.4664E-3	-6.0427E-6	-2.5285E-3	-2.3725E-3	9.8163E-4	-2.2269E-3	-1.3193E-3
19.35 H	0.4290	1.0685E-3	4.0082E-3	-2.9672E-3	1.4281E-3	1.7393E-3	-1.0247E-3	-2.2088E-3
22.235 V	0.5098	4.4664E-3	-6.0427E-6	-2.5285E-3	-2.3725E-3	9.8163E-4	-2.2269E-3	-1.3193E-3
37.0 V	0.3186	-1.5225E-3	1.7213E-3	-3.7164E-4	6.5607E-3	8.1213E-4	-1.7678E-3	-1.7250E-3
37.0 H	0.2622	-1.5095E-3	-1.9587E-5	5.0142E-4	6.8795E-4	5.7910E-3	-7.1539E-4	-2.1267E-3
Channel	**b_0**	**b_1**	**b_2**	**b_3**	**b_4**	**b_5**	**b_6**	
85.5 V	-0.9435	4.1137E-3	-7.0109E-6	1.5677E-2	-3.1055E-5	-6.5089E-3	1.4984E-5	
85.5 H	-0.9788	3.0851E-3	-5.2696E-6	7.4612E-3	-2.2772E-5	2.9755E-3	4.5324E-6	

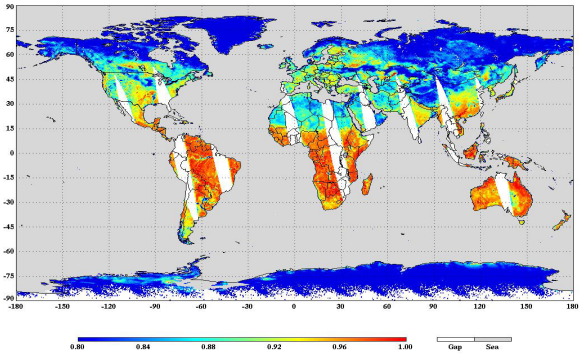

Figure 7: Same as Fig. 6 except for surface emissivity at 37.0 GHz H-Pol.

hurricane - the most dangerous part due to the additive effect of the wind speed and speed of the larger atmospheric flow. The relative calm eye and downdraft area between the spiral bands are also clearly shown. Note also that IWP displays a smooth transition along the coastal area. This illustrates that the cloud base temperatures are estimated fairly well and the uncertainties from land and ocean emissivity discontinuity are reduced to a minimum. However, it should be pointed out that this algorithm is more sensitive to precipitation-sized ice particles. Smaller ice particles whose diameters are less than 100 μm might not be well detected. Therefore, the retrieved IWP may be lower than in-situ observations.

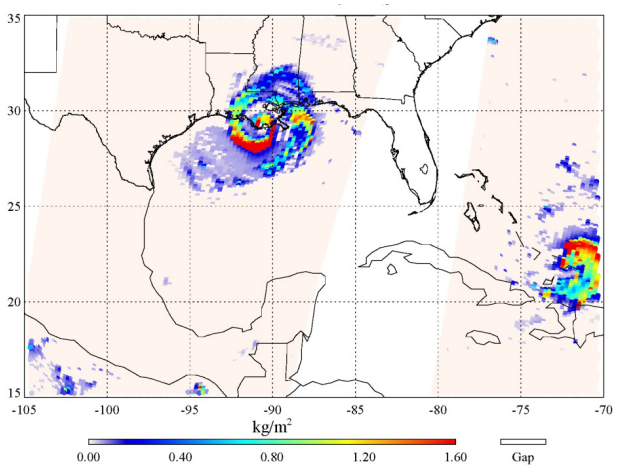

Figure 8: SSMIS derived ice water path for hurricane Gustav at the time of landfall on September 1, 2008.

4 Uses of SSMIS Data in Numerical Weather Prediction (NWP) Models

4.1 Fast Radiative Transfer Modeling Including Zeeman Effects

In a satellite data assimilation system or retrieval system, SSMIS brightness temperatures and their Jacobians (or gradient with respect to temperature and specific humidity) must be computed with a fast radiative transfer scheme[22,23]. For assimilation of SSMIS upper-level channels (19th to 24th channels), the Zeeman splitting effects which are dependent on the earth magnetic distribution[24] must be taken into account in the Community Radiative Transfer Model (CRTM). The SSMIS upper-air channels from 19th to 24th channels have a few Megahertz spectral passbands and center typically near the O2 magnetic dipole transition lines, designated with 7^+, 9^+, 15^+ and 17^+ [25]. Their weighting functions (WFs) peak in the upper stratosphere and mesosphere. Because of the Zeeman splitting effect, the energy received in some of the channels depends strongly on the geomagnetic field and its orientation with respect to the direction of observation. The theory of the microwave radiative transfer that takes the Zeeman Effect into account was developed by Lenoir[26,27]. Using Rosenkranz88[28], Han et al.[23] parameterized an averaged transmittance within an SSMIS frequency passband and predicted it with atmospheric temperature, geomagnetic field strength, and the angle between the geomagnetic field vector and the electromagnetic wave propagation direction. The coefficients of each predictor are trained with a line-by-line radiative transfer model that accurately computes the transmittance at each Zeeman splitting frequency. It is shown that SSMIS measurements agree well with the simulations that are based on the collocated atmospheric profiles from the COSPAR International Reference Atmosphere (CIRA) model (see Fig. 9). A Fortran program for fast and accurate computing of the Zeeman splitting effects has been developed and implemented as part of atmospheric gaseous absorption at microwave frequencies in CRTM.

4.2 SSMIS Data Assimilation in GFS

Today, satellite data that is routinely ingested in NCEP GFS include infrared and microwave sounding radiances from operational (e.g. NOAA/METOP HIRS/AMSU/MHS/IASI) and research platforms (e.g. Aqua AIRS), and derived products (e.g. AVHRR SST and Vegetation Fraction, MODIS wind, SBUV/2 ozone). Given its local observation times, atmospheric temperature and water vapor information from SSMIS are complementary to the measurements from NOAA/METOP satellites. The European Center for the Medium-range Weather Forecast (ECMWF) has demonstrated that the positive impact on global medium range forecasts of assimilating observations from three AMSUs on board NOAA-15, 16 and 17 was larger than any two combinations, especially for the North American forecasts. At the time of this 2003 experiment at ECMWF, three satellites provided a temporal refresh rate of almost 4 hours (the time crossing equator in its descending node is 7:30am, 10:00am, and 1:30pm for NOAA-15, 17, and 16 satellites). At any time, three satellites cover large oceanic areas crucial for global NWP forecasts which are insufficiently observed by a two satellite baseline. The forecasts over North America have benefited the most from the three AMSU instruments because they provide crucial information on up-stream weather systems over the northern Pacific Ocean, which is a void of conventional data. The impact of assimilating the observations of the F-16 SSMIS is tested in the NCEP GFS. The NCEP 3D-Var system, the Gridpoint Statistical Interpolation (GSI) system, is used to assimilate the GFS 6 hour forecast field with all the observations. The February 2010 GSI version is used to produce the analysis fields with a spectral resolution of T382 and 64 vertical sigma coordinate levels. The assimilation and forecast period covers August 1 to September 30, 2008.

It should be mentioned that the current GSI only assimilates clear radiances. For microwave sounding channels, the radiances are defined as clear data when the retrieved cloud liquid water content is smaller than 0.05 kg/m^2. Thus, this threshold can only filter out the measurements for the atmosphere having a liquid phase cloud. Globally, about 15%-20% of the microwave sounding radiances over oceans are not

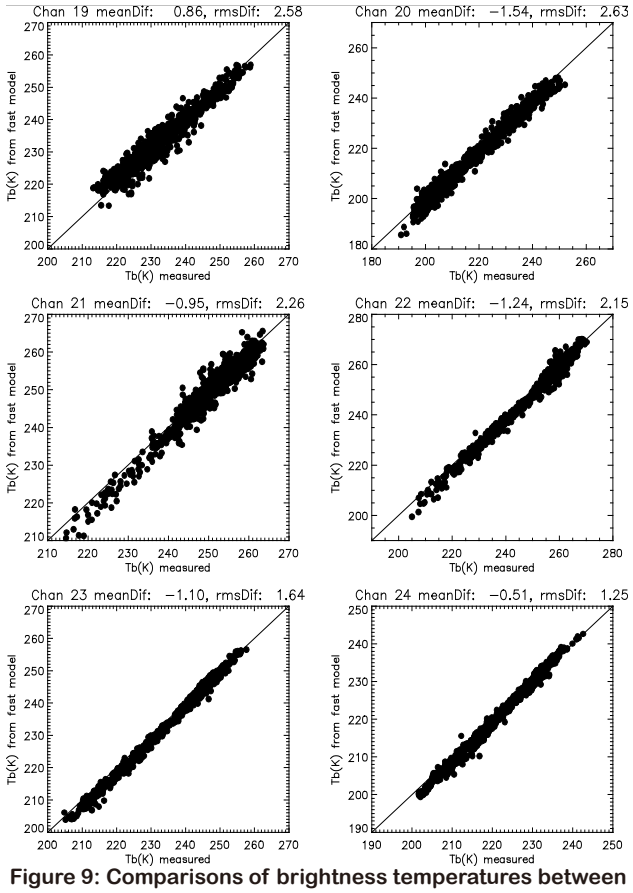

Figure 9: Comparisons of brightness temperatures between the fast model and observations. The mean difference (meanDif) and root-square-mean difference (rmsDif) are displayed on the top of each figure. A total of 1097 data points are included.

used in the data assimilation. Use of clouds and rain-affected microwave radiances in NWP systems is being actively pursued by the international community through advanced forward radiative transfer modeling and developments of tangent linear and adjoint models of NWP cloud and moisture physics.

It is important to point out that the current bias correction scheme in the GSI has some limitations[29] on SSMIS data assimilation. The bias correction scheme is in general needed and used to correct the inconsistency between observations and simulations from forecast model outputs. For an instrument that is well-calibrated, the bias correction will remove the errors of the radiances simulated from radiative transfer models. Thus, both accurate forward models and biased forecast model outputs can both lead to the biases in simulated radiances. In the GSI system, the several predictors such as atmospheric temperature lapse rate, cloud liquid water and instrument viewing angles are all used to predict the AMSU-A biases. Also, the same bias correction scheme is applied to the entire orbit of satellite measurements. Notice that for SSMIS LAS, biases are different between the ascending and descending nodes. Thus, for satellite orbit when entering the Southern Hemisphere, the bias correction is slightly revised with an additional offset.

As shown in Fig. 10, adding the SSMIS LAS to the GFS produces larger positive impacts, compared to the current baseline constellation from NOAA/METOP-A satellites. Using the SSMIS UPP dataset, with some correction of the regional dependent biases, significantly increases the impacts on global five-day forecasts as measured by the anomaly correlation coefficients of geopotential at the 500 hPa. Thus, the conical and cross-track scanning microwave sounders are both critical in the global observing systems.

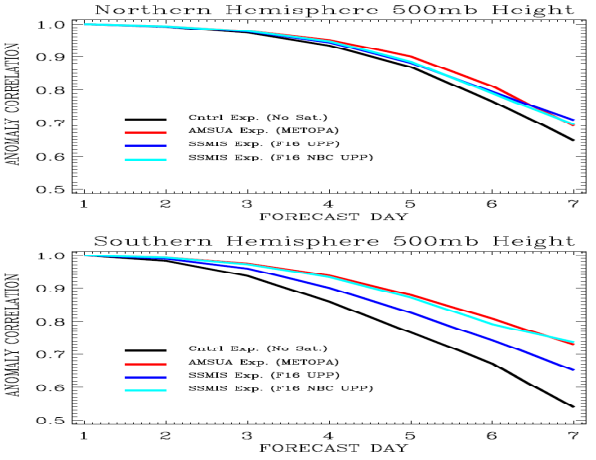

Figure 10: Impacts of assimilation of SSMIS LAS data on GFS medium-range forecasts with current and new bias correction schema. The control run uses all data except satellites.

4.3 Uses of SSMIS Cloudy Radiances in Hurricane Data Assimilation

In June 2006, GSI was released with the newly-developed CRTM. This marriage allows for assimilation of both clear and cloudy radiance from satellites into global forecast systems. Liu and Weng[11,12] tested assimilation of the SSMIS radiances using the GSI system. The core of the GSI system is a minimization of the cost function in a 3D-Var method that uses observations and priori or forecast information. The data assimilation system finds optimal analysis fields from forecast fields, conventional observations, some retrieval products as "observations", and satellite radiances under dynamic constraints following a set of physical laws. It is shown that the initial temperature fields at 200 hPa for the "control-run" show a typical warm core (see Fig.11a) at the central area of hurricanes. But the warm core is very smooth and weak due to the coarse spatial resolution of the global analysis and the absence of cloud radiance assimilation. The structure and strength of the warm core in the new initial temperature field at 200 hPa is much improved compared with the "test-run" (see Fig.11b). The new initial field displays the vortex structure and has the warmest temperature at the hurricane center. The initial temperature field at 850 hPa for the "control-run" is also very smooth (see Fig.11c). The new initial temperature field at 850 hPa for the "test-run" shows the warm

core in the central area and the cold temperature associated with the spiral rain band (see Fig.11d). Overall, the temperature field of the "control run" is weak and lacks the detailed features associated with the cumulus clouds; the new data assimilation with the "test-run" preserves the fine structure of the clouds within the hurricane.

4.4 SSMIS Data Assimilation in Stratosphere

In order to quantify the effect of SSMIS radiances on stratospheric temperatures, we compare the temperature fields of 6-hour forecasts with those of our new analysis (hereafter referred to as test). To quantify the pure impact of using SSMIS data on the analysis, the new analysis only utilizes the forecast fields and SSMIS brightness temperatures for stratospheric temperatures in the NCEP GSI system. It is the first time for the SSMIS brightness temperatures being utilized for the stratospheric temperature analysis in the NCEP GSI system. The differences in stratospheric temperatures between the 6-hour forecast and new analysis are plotted in Figure 12. In comparison to the 6-hour forecast, the stratospheric temperature from the test run is warmer, reducing the cold bias of the forecast. The area of the warm increment for the temperature at 100 hPa is very small, indicating an accurate 6-hour forecast at that level. Significant warm increments in the temperature of the middle and lower stratosphere (30 - 70 hPa) is seen in the test run. The 30 - 70 hPa atmospheric layer contains the peak in the ozone concentration and is the region where ozone depletion occurs. The warm increment of about 2 degrees in the temperature of the lower stratosphere from the new data analysis is consistent with the reported cold bias in NCEP analyses. The relatively small area of warm increment in the temperature at 10 hPa may again indicate an accurate forecast. Figure 12f shows a comparison of the temperature profiles of the 6-hour forecast (red line), radiosonde (green line), and new analysis (black line). The new analysis shows an improvement in the temperature profile between 30 and 70 hPa. The differences among the three datasets at 10 hPa may be due to the uncertainty of the radiosonde data at high-pressure levels. Overall, the new data analysis using SSMIS observations improves the accuracy of the stratospheric temperatures. The result of this study indicates that assimilation f SSMIS observations will benefit NWP forecasts. It should be mentioned that the entire three-dimensional temperature field is adjusted in radiance assimilation - even the part of the filed covered by satellite measurements - which is the essential difference between radiance assimilation and the one-dimensional retrieval.

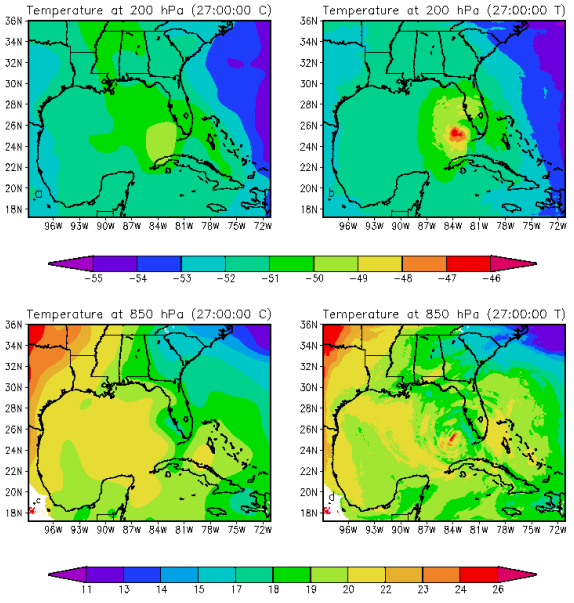

Figure 11: The initial temperature field at 200 hPa for (a) the "control-run" , (b) "test-run", and at 850 hPa for (c) the "control-run" and (d) "test-run".

5 Impacts of SSMIS on Climate Monitoring

As previously mentioned, the SSM/I time series dates back to July 1987; thus, nearly 20 years of critical information related to the Earth's climate have been derived using a series of simple, yet, reliable algorithms[1,3,17,30]. These products are used by a host of government and academic institutions to support both operational climate monitoring and to advance climate research. As we transition into the SSMIS era, it is essential that this time series continues into the future and that the transitions between spacecraft and sensors are "seamless" so that artificial trends are eliminated. Although beyond the scope of this paper, NOAA/NESDIS has begun an effort under its scientific data

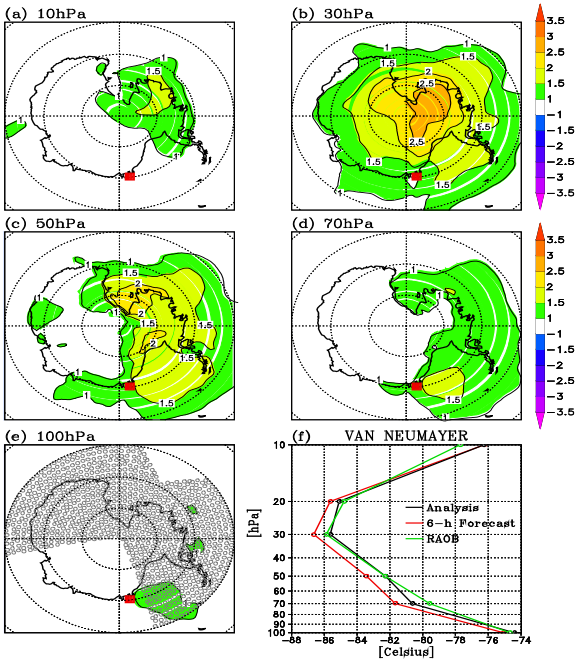

Figure 12: Differences of stratospheric temperatures between new analyses and 6-hour forecasts valid at 1200 UTC June 29, 2006. The Van Neumayer station is indicated by the red colored square. The black circles are footprints of the SSMIS measurements. The stratospheric temperature profiles from the 6-hour forecast, radiosonde, and new analysis for the time are provided in (f).

stewardship (SDS) program to generate climate data records (CDR's; see [31]) from the SSM/I and SSMIS. This effort will involve a robust characterization of each sensor in the time series, including both inter- and intra-satellite calibrations that are essential in creating meaningful CDR's.

To illustrate the potential use of the SSMIS in global climate monitoring, Fig. 13 shows "typical" uses of the products using the legacy algorithms. The figure includes maps of the monthly mean total precipitable water (TPW) for October 2005 and October 2006, their interannual difference, and sea-surface temperature (SST) for October 2006. The interannual differences of TPW (Fig. 13c) reveal some interesting features that are consistent with the SST anomalies (Fig. 13d). The main difference between 2005 and 2006 is that warm SST conditions developed in 2006 in response to an El Nino event, and this is clearly depicted by the general increase in TPW values in October 2006 in the equatorial Pacific, surrounded by regions of decreased TPW, which are consistent with decreases in SST. A long-term climatology of such products is feasible by extending the 20-year SSM/I time series with SSMIS data over the next decade.

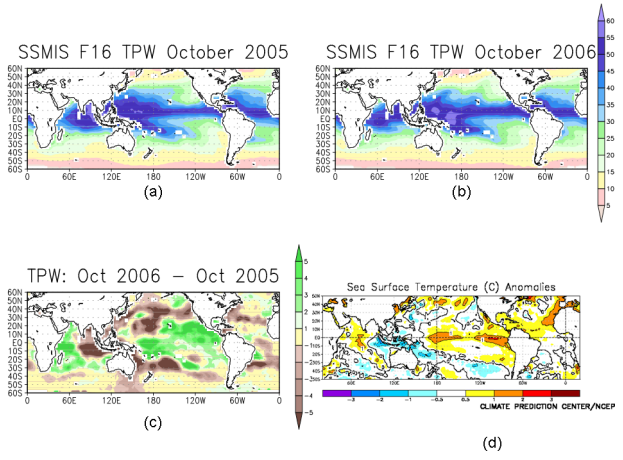

Figure 13: F-16 SSMIS derived TPW for (a) October 2005 and (b) October 2006 (unit: mm). The interannual difference is provided in (c) while the sea surface temperature anomalies (unit: deg C) for October 2006 are provided in (d) (Courtesy of NOAA/CPC).

6 Summary and Conclusions

Since the DMSP launched its F-16 satellite with the SSMIS on board, the NWP user community has developed methods to detect and mitigate the SSMIS radiance anomalies due to thermal emission of the main reflector and calibration target count perturbations. The NWP data assimilation system outputs are used to produce global simulations of brightness temperatures that are then compared with SSMIS measurements. While this comparison is different from direct calibration, some fundamental issues such as antenna emission and warm load intrusion from solar and spacecraft radiation are characterized. Using the unified preprocessing package that was developed by NRL and MetOffice, the SSMIS data are now routinely assimilated into NOAA's GFS. It is shown that the impacts of the SSMIS lower atmospheric sounding (LAS) channels on global medium-range forecasts are very similar to those of the AMSU instrument. The SSMIS cloudy radiances from these channels also produce realistic warm core structures of hurricanes. Since SSMIS can probe up to 100 km altitude, the impacts of SSMIS upper atmospheric sounding (UAS) channels are unique and much larger than those from other observing instruments. In addition, SSMIS imager channels are also being used to generate monthly and annually averaged retrieval products that could be linked to the previous SSM/I time series for studying climate and climate change.

Acknowledgement and Disclaimer: This work was supported by Chinese Ministry of Science and Technology under project 2010CB951600 and NOAA/NESDIS satellite Cal/Val program. The views expressed in this publication are those of the authors and do not necessarily represent those of NOAA.

REFERENCES

[1] Ferraro R R, Weng F, Grody N, Basist A. An eight year (1987-1994) time series of rainfall, clouds, water vapor, snow and sea ice derived from SSM/I measurements. Bull. Amer. Meteor. Soc., 1996,77: 891-905.

[2] Alishouse J C, Snyder S A, Vongsathorn J, Ferraro R R. Determination of Oceanic Total Precipitable Water from the SSM/I. IEEE Trans. Geosci Remote Sens., 1990, 28:811-816.

[3] Weng F, Grody N C. Retrieval of cloud liquid water using the special sensor microwave imager (SSM/I). J. Geophys. Res., 1994, 99(25):535-25, 551.

[4] Boucher D, Poe G, Coauthors. Defense Meteorological Satellite Program Special Sensor Microwave Imager Sounder (F-16) Calibration/Validation Final Report, November, 2005.

[5] Northrop Grumman. Algorithm and Data User Manual (ADUM) for the Special Sensor Microwave Imager/Sounder (SSMIS). Report 12621. Azusa, California: Northrop Grumman Corporation: Space Systems Division, 2002.

[6] Swadley S, Poe G, Baker N, et al. Calibration Anomalies and Radiance Assimilation Correction Strategies for the Defense Meteorological Satellite Program (DMSP) Special Sensor Microwave Imager Sounder (SSMIS). 15th International TOVS Study Conference, Maratea, IT, 2006.

[7] Swadley S, Poe G, Baker N, et al. SSMIS radiance assimilation, calibration anomaly mitigation and early results from F-18, presented at 11th Specialist Meeting on Microwave Radiometry and Remote Sensing of the Environment, 2010.

[8] Yan B, Weng F. Assessments of F-16 Special Sensor Microwave Imager and Sounder Antenna Temperatures at Lower Atmospheric Sounding Channels. Advances in Meteorology, 2009: doi: 10. 1155.

[9] Bell W, English S, Candy B, et al. The assimilation of SSMIS radiances in NWP models. IEEE Trans. Geoscience and Remote Sensing, 2008,46: 884-900.

[10] Yan B, Weng F. Intercalibration between Special Sensor Microwave Imager and Sounder (SSMIS) and Special Sensor Microwave Imager (SSM/I). IEEE Trans. Geosci. Remote Sens, 2008, 46: 984-995.

[11] Liu Q, Weng F. Detecting Warm Core of Hurricane from the Special Sensor Microwave Imager Sounder. Geophys. Res. Letters, 2006, 33:L06817, doi:10.1029/2005GL025246.

[12] Liu Q, Weng F. Radiance assimilation in studying Hurricane Katrina. Geophys. Res. Lett., 2006, 33: L22811, doi:10.1029/2006GL027543.

[13] Liu Q, Weng F. One-dimensional retrieval algorithm of temperature, water vapor, and cloud water profiles from advanced microwave sounding unit (AMSU). IEEE Geosci. Remote Sensing, 2005, 43(5): 1087-1095.

[14] Boukabara S, Weng F, Liu Q. Passive microwave remote sensing of extreme weather events using NOAA-18 AMSUA and MHS.

IEEE Trans Geos Remote Sens, 2007, 45: 2228-2246.
[15] Deblonde G, English S J. Evaluation of the FASTEM-2 fast microwave oceanic surface emissivity model, Tech. Proc. ITSCXI Budapest , 2026 Sept 2000, 2001: 67-78.
[16] Weng F, Grody N C. Retrieval of liquid and ice water content in atmosphere using the Special Sensor Microwave/Imager (SSM/I). Microwave Radiometer and Remote Sensing of Environment. X. Solminili, Ed., 1994, VSP: 281-295.
[17] Ferraro R R. SSM/I derived global rainfall estimates for climatological applications. J. Geophys. Res., 1997, 102(16): 715-16, 735.
[18] Weng F, Grody N C. Physical retrieval of land surface temperature using the special sensor microwave imager. Journal of Geophysical Research-Atmospheres, 1998, 103: 8839-8848.
[19] Sun N, Weng F. Evaluation of Special Sensor Microwave Imager and Sounder (SSMIS) Environmental Data Record. IEEE Trans. Geosci. Remote Sens, 2008, 46: 1006-1016.
[20] Weng F, Grody N C. Retrieval of ice cloud parameters using a microwave imaging radiometer. J. Atmos., Sci., 2000, 57: 1069-1081.
[21] Zhao L, Weng F. Retrieval of ice cloud parameters using the Advanced Microwave Sounding Unit (AMSU). J. Appl. Meteorol., 2002, 41: 384-395.
[22] Weng F, Han Y, van Delst P, Liu Q, Yan B. JCSDA Community radiative transfer model (CRTM). Technical Proceedings of Fourteenth International ATOVS Study Conference, Beijing, 2005.
[23] Han Y, Weng F, Liu Q, van Delst. A fast radiative transfer model for SSMIS upper-air sounding channels. J. Geophys. Res., 2007, 112, D11121.doi: 10.1029/2006JD008208.
[24] Stogryn A. The magnetic field dependence of brightness temperature at frequencies near the O_2 microwave absorption lines. IEEE Trans. Geosci. Remote Sens, 1989, 27: 279-289.
[25] Rosenkranz P, Tewarson N C, Singh A, Engels W. Differential hygienic behavior towards Varroa jacobsoni in capped worker brood of Apis cerana depends on alien scent adhering to the mites. J. Apic. Res. 1993, 32: 89-93.
[26] Lenoir W B. Propagation of partially polarized wave in a slightly anisotropic medium. J. Appl. Phys., 1967, 38: 5283-5290.
[27] Lenoir W B. Microwave spectrum of molecular oxygen in the mesosphere. J. Geophys. Res., 1968, 73: 361-376.
[28] Rosenkranz P W, Staelin D H. Polarized thermal microwave emission from oxygen in the mesosphere. Radio Science, 1988, 23: 721-729.
[29] Derber J, Wu W-S. The use of TOVS cloudcleared radiances in the NCEP SSI analysis system. Mon. Wea. Rev., 1998, 126: 2287–2299.
[30] Huffman G J, Adler R F, Arkin P, et al. The Global Precipitation Climatology Project (GPCP) combined precipitation data set. Bull. Amer. Meteor. Soc., 1996, 78: 5-20.
[31] Robinson J, Isidore M, Marguerite M A, Öhman M C, Payet R J. Spatial and temporal distribution of reef fish spawning aggregations in the Seychelles – An interview based survey of artisanal fishers. Western Indian Ocean J. Mar. Sci., 2004, 3: 63-69.

卫星专用传感器微波成像仪/探测仪（SSMIS）观测资料在天气和气候研究中的应用

Weng F[1,2], Zou X*[3,4], Yan B[2], Han Y[1,2], Liu Q[2,5]

(1 美国国家海洋和大气管理局/国家环境卫星、数据与信息服务部/卫星应用与研究中心，美国 2 卫星数据同化中心，美国 3 南京信息工程大学数据同化研究与应用中心，南京，中国 4 佛罗里达州立大学，地球海洋大气科学系，美国 5 IMSG公司，美国)

摘要： 2003年10月18日，美国国防气象卫星计划成功发射搭载了专用传感器微波成像仪/探测仪的F–16卫星。然而由于天线自身热辐射和校准暖黑体的不稳定，第一个专用传感器微波成像仪/探测仪出现了一些重要的异常观测。美国海军实验室与美国国家海洋和大气管理局(NOAA)分别开发了两种算法来订正这些异常值。剔除了定标异常值后，专用传感器微波成像仪/探测仪资料目前在探空数据产品反演和资料同化中发挥了更加显著的作用。NOAA利用专用传感器微波成像仪已有算法生成了专用传感器微波成像仪/探测仪成像仪产品。此外，一些新开发的算法可以从专用传感器微波成像仪/探测仪资料中提取出云和降水的信息。在云冰云水的反演算法中，亮温是与云冰云水路径和粒子的平均直径相关的。利用一维变分反演系统，同时反演出了多数大气和地表条件下的大气温度、湿度以及水凝物的垂直廓线。在各种天气形势下，由专用传感器微波成像仪/探测仪资料反演得到的温度和湿度廓线的均方根误差通常分别小于2K和15%。为了同化专用传感器微波成像仪/探测仪资料，还发展了新的质量控制和偏差订正方法。在NOAA的全球预报系统中同化了专用传感器微波成像仪/探测仪资料后，对提高全球中期数值预报水平产生了中性和较小的正效果。

（上接13页）

40th Anniversary of Fengyun Meteorological Satellites: Evolution in View of the International Development

Yang Jun, Xu Jianmin, Dong Chaohua

(National Satellite Meteorological Center, China Meteorological Administration, Beijing 100081)

Abstract: With 40 years' huge efforts, China has successfully developed both polar and geostationary meteorological satellite series, and put them into operational use. This article reviews the significant historical events along with the stages of meteorological satellite development in the world, outlines the development of Chinese Fengyun meteorological satellites in the scope of international views, and compares Fengyun's technical level with that in advanced countries. In addition, it briefly introduces the applications of meteorological satellite data in weather, climate, natural disasters and environmental monitoring, and in the agriculture service.